Salt-Dependent RNA Pseudoknot Stability: Effect of Spatial Confinement

Chenjie Feng[1], Ya-Lan Tan[1], Yu-Xuan Cheng[1], Ya-Zhou Shi[2]* and Zhi-Jie Tan[1]*

[1] Key Laboratory of Artificial Micro and Nano-structures of Ministry of Education, Center for Theoretical Physics, School of Physics and Technology, Wuhan University, Wuhan, China, [2] Research Center of Nonlinear Science, School of Mathematics and Computer Science, Wuhan Textile University, Wuhan, China

Macromolecules, such as RNAs, reside in crowded cell environments, which could strongly affect the folded structures and stability of RNAs. The emergence of RNA-driven phase separation in biology further stresses the potential functional roles of molecular crowding. In this work, we employed the coarse-grained model that was previously developed by us to predict 3D structures and stability of the mouse mammary tumor virus (MMTV) pseudoknot under different spatial confinements over a wide range of salt concentrations. The results show that spatial confinements can not only enhance the compactness and stability of MMTV pseudoknot structures but also weaken the dependence of the RNA structure compactness and stability on salt concentration. Based on our microscopic analyses, we found that the effect of spatial confinement on the salt-dependent RNA pseudoknot stability mainly comes through the spatial suppression of extended conformations, which are prevalent in the partially/fully unfolded states, especially at low ion concentrations. Furthermore, our comprehensive analyses revealed that the thermally unfolding pathway of the pseudoknot can be significantly modulated by spatial confinements, since the intermediate states with more extended conformations would loss favor when spatial confinements are introduced.

Keywords: coarse-grained model, RNA pseudoknot, spatial confinement, salt effect, stability

INTRODUCTION

RNAs have been shown to perform many crucial biological functions, including the regulation of gene transcription and translation and the catalysis of RNA splicing (Serganov and Patel, 2007; Sashital and Doudna, 2010). An RNA pseudoknot is a very common RNA structure motif and can play important roles in many cellular functions (e.g., stimulating programmed−1 ribosomal frameshifting), which are directly related to the folding stability and conformational changes of the pseudoknot (Giedroc et al., 2000; Staple and Butcher, 2005). Accordingly, to determine 3D structures and stability of RNA pseudoknots is essential to understand and utilize their related functions (Giedroc et al., 2000; Giedroc and Cornish, 2009; Wang et al., 2015a).

Although experimental methods, such as X-ray crystallography, nuclear magnetic resonance spectroscopy, and cryo-electron microscopy, can be used to determine the structures of RNAs including pseudoknots, the structures in Protein Data Bank (PDB; https://www.rcsb.org) are still limited due to the high cost of the experimental measurements (Hajdin et al., 2010; Rose et al., 2011; Shi et al., 2014b; Schlick and Pyle, 2017). To complement the experiments, some computational models/methods (e.g., FARNA, MC-Fold/MC-Sym, Vfold, iFoldRNA, 3dRNA, RNAComposer,

SimRNA, oxRNA, HiRE-RNA, and pk3D) have been developed for predicting RNA 3D structures (Cao and Chen, 2005; Ding et al., 2008; Parisien and Major, 2008; Zhang et al., 2009; Das et al., 2010; Popenda et al., 2012; Zhao et al., 2012; He et al., 2013, 2015, 2019; Kim et al., 2014; Liwo et al., 2014, 2020; Sulc et al., 2014; Cragnolini et al., 2015; Wang et al., 2015a,b; Boniecki et al., 2016; Dawson et al., 2016; Li et al., 2016, 2018; Tan et al., 2019). Most of these models/methods are primarily designed to predict folded structures and cannot predict the stability of RNAs, especially in ion solutions (Shi et al., 2014b; Dawson et al., 2016; Schlick and Pyle, 2017), whereas the structural stability of RNAs can be very sensitive to ion conditions due to their polyanionic nature (Das et al., 2005; Draper et al., 2005; Tan and Chen, 2007, 2011; Qiu et al., 2010; Lipfert et al., 2014; Wang et al., 2018, 2020; Meng et al., 2020). Recently, to predict the 3D structures, stability, and flexibility of RNAs in ion solutions from sequences, we have developed a new coarse-grained (CG) model, and the model has been validated for extensive RNA hairpins, kissing complex, and pseudoknots over a wide range of monovalent/divalent ion concentrations (Shi et al., 2014a, 2015, 2018; Jin et al., 2018, 2019).

Furthermore, RNAs are generally residing in crowded cellular microenvironment with many other macromolecules, and the volume percentage of macromolecules could take up to ∼40% (Leamy et al., 2016). Recent experiments showed that spontaneous folding of RNAs and proteins in crowded environment can be substantially different from that observed in *in vitro* experiments, usually conducted only in the presence of small molecular weight buffers (Kilburn et al., 2013, 2016; Paudel and Rueda, 2014; Leamy et al., 2017; Yamagami et al., 2018). For example, small angle X-ray scattering (SAXS) measurements on ribozymes in the presence of polyethylene glycol indicated that molecular crowding can apparently stabilize the compaction of folded structures and favor the transition from unfolded state to folded state at low ion concentrations (Kilburn et al., 2010, 2013, 2016). Thermal denaturation and SAXS studies also showed that crowding agents can promote the tRNA folding cooperativity by stabilizing its tertiary structure in physiological ion concentrations (Leamy et al., 2017; Yamagami et al., 2018). Meanwhile, several theoretical studies have also been performed to investigate how molecular crowding influences RNA stability (Denesyuk and Thirumalai, 2011; Tan and Chen, 2012; Dupuis et al., 2014; Feig et al., 2017). For example, Denesyuk and Thirumalai used a three-interaction-site CG model to simulate the switch from hairpin to pseudoknot conformations in the human telomerase RNA under different crowded environments and showed that crowders could enhance the stability of pseudoknot relative to hairpin state through reducing the population of extended conformations in the unfolded state (Denesyuk and Thirumalai, 2011). Due to the salt-dependent compactness of unfolded states of RNAs, the crowding effect could be very sensitive to ion conditions. However, previous works for RNAs under crowded environment were mainly focused on high salt conditions, and thus the electrostatic interactions are minimally present. Very recently, Yu et al. developed a new statistical mechanical treatment to predict the effect of molecular crowding on ion–RNA interactions, but the

model is limited for the folded RNA conformations and could not be applicable for RNA folding (Yu et al., 2016). Therefore, how macromolecular crowding impacts the salt-dependent 3D structures and stability of RNAs is still elusive.

In this study, we used a typical RNA pseudoknot as a paradigm to systematically investigate the effect of spatial confinement on the 3D structures, stability, and unfolding pathways of RNAs in ion solutions. First, we employed our CG model to predict 3D structures and stability of the RNA pseudoknot under various spatial confinements over a wide range of ion concentrations. Afterward, we examined the effect of spatial confinement on the salt-dependent 3D structures and stability for the RNA pseudoknot. Finally, we made comprehensive analyses on the effect of spatial confinement on the thermally unfolding pathways for the RNA pseudoknot in different ion solutions.

MATERIALS AND METHODS

The CG Structure Model and Force Field

To predict the 3D structures and stability of RNAs in various ion solutions, we have developed a new CG model with involving the effects of ions (Shi et al., 2014a, 2015, 2018; Jin et al., 2018, 2019). In the model, each nucleotide is represented by three beads, which represent the three atom groups: phosphate group (P), sugar ring (C), and base (N), respectively. The P and C beads within the backbone are placed at the P and C4′ atoms, respectively, and the N beads are placed at N9 atoms for purine or N1 atom for pyrimidine (Shi et al., 2014a). The interactions between the CG beads are composed by eight energy terms. Namely, for a given RNA conformation, the effective potential energy (U) is given by:

$$U = U_b + U_a + U_d + U_{exc} + U_{bp} + U_{bs} + U_{cs} + U_{el}, \quad (1)$$

where the first three terms are bonded potentials, and the remaining terms are non-bonded potentials to describe various pairwise non-bonded interactions. The function forms and the determination of the parameters for the eight terms in Equation (1) have been described in detail in Shi et al. (2014a) and can also be found in **Supplementary Material**. The energy terms were described very briefly as follows.

The bond length energy U_b, bond angle energy U_a, and dihedral energy U_d account for the connectivity and angular rotation for an RNA chain, and their parameters have two sets: Para$_{nonhelical}$ for single strands/loops in RNA folding process and Para$_{helical}$ for helical stems only in structure refinement, which are derived from the statistical analysis of the 3D structures of RNAs in the PDB (https://www.rcsb.org) (Rose et al., 2011). The U_{exc} in Equation (1) represents excluded volume interactions between two CG beads, and the P, C, and N beads are treated as spheres with van der Waals radii (r) of 1.9 Å, 1.7 Å, and 2.2 Å, respectively. The U_{bp}, U_{bs}, and U_{cs} in Equation (1) are the base-pairing (between Watson–Crick and wobble base pairs), base-stacking (between nearest-neighbor base pairs), and coaxial stacking (between two discontinuous neighbor helices) interactions, respectively, and the strength of them was derived from sequence-dependent thermodynamic parameters and the

corresponding experimental data (Xia et al., 1998; Spasic et al., 2018). The last term U_{el} in Equation (1) is an electrostatic potential corresponding to electrostatic interactions between phosphate groups (a charge of $-e$ for each P bead at its center), which are ignored by most existing predictive models for RNA 3D structures (Hajdin et al., 2010; Rose et al., 2011; Shi et al., 2014b; Schlick and Pyle, 2017). The U_{el} is taken into account through the combination of the Debye–Hückel approximation, the concept of counterion condensation (CC) (Manning, 1978), and the tightly bound ion (TBI) model (Tan and Chen, 2007, 2010, 2011), and the potential can well-capture the contribution of monovalent/divalent ions to RNA 3D structures (Shi et al., 2015; Jin et al., 2019).

Material and Spatial Confinement

In this work, we used the 34-nucleotide RNA pseudoknot from mouse mammary tumor virus (MMTV; PDB code: 1rnk; sequence: 5′-GGCGCAGUGGGCUAGCGCCACUCAA AAGGCCCAU-3′; https://www.rcsb.org) as a model RNA to investigate the crowding effect on RNA folding, considering the biological role of the MMTV pseudoknot in stimulating programmed -1 ribosomal frameshifting in the ribosome tunnel (Shen and Tinoco, 1995). The sequence and experimental structures are shown in **Figure 1**. As shown in **Figure 1**, the pseudoknotted structure is formed when a sequence of nucleotides within a single-stranded loop region forms base pairs with a complementary sequence outside that loop, and it includes two stems (Stem 1 and Stem 2) and three loops (Loop 1, Loop 2, and Loop 3).

Although the interactions between macromolecule crowders and RNAs could be very complex, experimental and theoretical studies have shown that when the crowding particles are much bigger and heavier than the target RNA (e.g., RNA pseudoknots in the ribosome tunnel), the macromolecular crowding effects can be approximated by a spatial confinement, the shape and dimensions of which would depend on the crowding concentration (Cheung et al., 2005; Mittal and Best, 2008; Zhou et al., 2008; Qin and Zhou, 2014; Hori et al., 2016; Feig et al., 2017). For example, Cheung et al. used a spherical cavity to mimic the effect of crowding and obtained the mapping between crowding and effective confinement (Cheung et al., 2005):

$$R_s = \left(\frac{4\pi}{3\varphi_c}\right)^{\frac{1}{3}} R_c, \qquad (2)$$

where R_S is the radius of spherical pore, and R_c is the radius of the macromolecular crowding agents. φ_c in Equation (2) is the volume fraction of crowding agents. Recently, Mittal and Best (2008) examined the effect of different confinement geometries (e.g., planar, cylindrical, and spherical) on protein-folding thermodynamics and kinetics and found that the stabilization of the folded state relative to bulk conditions was independent of the geometry of confinement. Thus, here, we applied spherical cavity with different spherical radii R_S [e.g., 35 Å, 45 Å, and 55 Å designed based on Equation (2)] to mimic the crowding effects on the folding of MMTV pseudoknot over a wide range of Na^+ concentrations [(Na^+)]; see **Figure 1A**. Although the short-range

repulsive interactions between atoms of macromolecules and the inner walls of sphere are often mimicked by the potential of $\left(\frac{a}{r}\right)^{12}$ (Klimov et al., 2002), since there is no significant difference between the potential and an ideal hard-wall potential, in this work, the interaction between the spherical cavity and the RNA pseudoknot was still approximate by a purely repulsive hard-wall potential for simplicity (Klimov et al., 2002; Tan and Chen, 2012):

$$U_{RC} = \begin{cases} \infty & if \ d > R_s - r \\ 0 & if \ d \le R_s - r \end{cases}, \qquad (3)$$

where d is the distance between the CG beads and spherical cavity center, and r is the van der Waals radius of the CG beads.
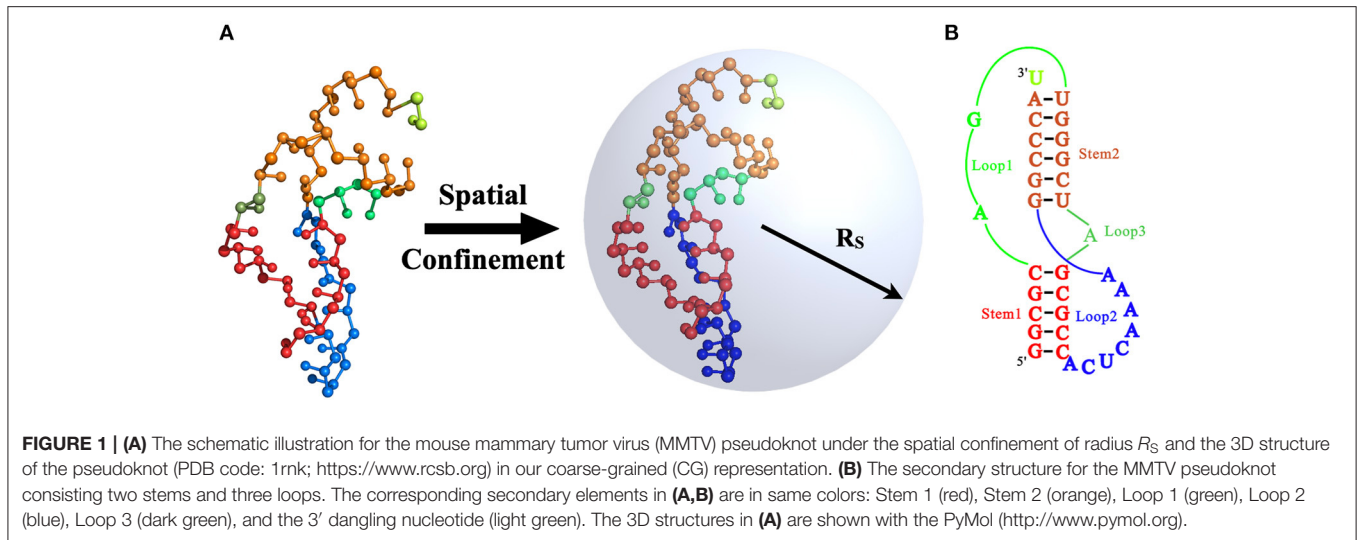
Simulation Algorithm

To improve the efficiency of conformational search, we used the Monte Carlo (MC)-simulated annealing algorithm with pivot move to predict the 3D structures for the MMTV pseudoknot at different conditions [e.g., temperature, (Na^+) and radius of spherical confinement R_S] from its sequence. The simulation is performed from high temperature (e.g., 400 K) to the target temperature (e.g., 298 K) with gradual cooling steps. At each temperature, RNA conformational changes are accomplished *via* the translations/pivot moves and the Metropolis criterion until the system reaches enough equilibrium (Shi et al., 2014a, 2018). The equilibrium conformations of the MMTV pseudoknot at each temperature under given conditions are saved to analyze the effect of spatial confinement on salt-dependent 3D structures, stability, and unfolding pathway of the RNA.

RESULTS AND DISCUSSION

To systematically evaluate how spatial confinement influence RNAs, we first employed the CG model to predict the 3D structures of the MMTV pseudoknot at different spatial confinements, ion conditions and temperatures. Afterward, we further examined the effect of spatial confinement on the stability and unfolding pathway of the pseudoknot over a wide range of ion concentrations.

Effect of Spatial Confinement on Salt-Dependent Structures

First, based on the sequence, we predicted 3D structures of the MMTV pseudoknot at 25°C and 1 M [Na^+]. As shown in **Supplementary Figure 1**, the system reaches enough equilibrium after a number of temperature-annealing MC steps (e.g., $\sim 3 \times 10^8$), and all the conformations in the following simulations are the structures predicted by the present model. The predicted mean radius of gyration R_g of the pseudoknot is $\sim$15.7 Å, which is very close to that (15.1 Å) of the experimental structure (PDB code: 1rnk; https://www.rcsb.org), and the mean and minimum root-mean-square deviations (RMSDs) between predicted structure ensemble and experimental structure are $\sim$4.6 and 3.2 Å, respectively, which suggest that the present model can give reliable prediction for the 3D structure of the RNA pseudoknot in the absence of spatial confinement; refer Shi et al. (2018).

FIGURE 1 | (A) The schematic illustration for the mouse mammary tumor virus (MMTV) pseudoknot under the spatial confinement of radius R_S and the 3D structure of the pseudoknot (PDB code: 1rnk; https://www.rcsb.org) in our coarse-grained (CG) representation. **(B)** The secondary structure for the MMTV pseudoknot consisting two stems and three loops. The corresponding secondary elements in **(A,B)** are in same colors: Stem 1 (red), Stem 2 (orange), Loop 1 (green), Loop 2 (blue), Loop 3 (dark green), and the 3′ dangling nucleotide (light green). The 3D structures in **(A)** are shown with the PyMol (http://www.pymol.org).

Afterward, we predicted 3D structures for the pseudoknot at different [Na$^+$]s and temperatures under various spatial confinements (e.g., R_S from 35 to 55 Å). To obtain enough equilibrium conformations, we ran the simulations for a long time (e.g., ~7 × 10^8 MC steps for $R_S = \infty$ Å); see **Supplementary Figure 2**. The calculated R_gs and fractions fs of formed base pairs for the pseudoknot at different conditions are shown in **Figure 2** and **Supplementary Figure 2**. Here, the fractions of formed base pairs f is calculated by:

$$f = \frac{\frac{1}{t}\sum_t N_{bp}(t)}{N_{bp}}, \tag{4}$$

where $N_{bp}(t)$ is the total number of formed base pairs at MC step t, and N_{bp} is the number of predicted native base pairs at room temperature [e.g., ~10 bp at 1 M (Na$^+$)].

As shown in **Figure 2** and **Supplementary Figure 2**, we found that the spatial confinement has very slight effect on the folded structures at low temperature (e.g., 20°C), but has a considerable compacting effect on (partially) unfolded structures at high temperature (e.g., 120°C). For example, at 1 M [Na$^+$] and 20°C, R_g of the RNA (~16.1 Å) within the spatial confinement of radius $R_S = 35$ Å is almost the same as that (~16.1 Å) without the spatial confinement, whereas at 120°C, the confinement of $R_S = 35$ Å can compact the structure of the RNA by ~12.3 Å in R_g; see also in **Supplementary Figure 4**. This structure compacting effect is consistent with the recent works (Denesyuk and Thirumalai, 2011; Kilburn et al., 2013) and to directly understand this, we calculated the maximum distance R_{max} between CG beads and the centroid of the conformations at $R_S = \infty$ Å; see **Figure 3**. As shown in **Figure 3A**, the mean R_{max} for unfolded structures at 1 M [Na$^+$] and 120°C is ~61 Å, which is much larger than confinement radii R_Ss used in this work (e.g., 35 Å), whereas R_{max} (~26 Å) for folded structures at 20°C is smaller than the used R_Ss. Thus, the spatial confinement can compact (partially) unfolded

structures more significantly than folded ones, since (partially) unfolded structures are apparently more extended.

Furthermore, we examined the effect of spatial confinement on salt dependence of the pseudoknot structure compactness, since ions such as Na$^+$ can promote RNA folding and favor folded compact structures (Draper et al., 2005; Tan and Chen, 2010, 2011; Lipfert et al., 2014). As shown in **Figures 2A–C**, the spatial confinement weakens the dependence of structure compactness on salt concentration over the wide range of temperatures, especially for (partially) unfolded structures. For example, in the absence of spatial confinement, the decrease of R_g due to the increase of [Na$^+$] from 0.01 to 1 M are ~9.8 and 2.6 Å at 120 and 20°C, respectively, which are visibly larger than those (~4.2 and 1.6 Å at 120 and 20°C, respectively) in the presence of the confinement of $R_S = 35$ Å. This is because that the spatial confinement can spatially constraint the conformational space for an RNA inside, and such effect is more severe for more extended structures (e.g., at lower salt or at higher temperature); see also **Figures 3B–D**. Thus, the structure compactness of an RNA becomes more weakly dependent on salt concentration in a stronger spatial confinement.

Corresponding to the above-described effect on structure compactness, a spatial confinement would promote the formation of base pairs through its compacting effect as shown in **Figures 2D–F**. Such effect of promoting base pairing appears rather weak for the two limit cases of high salt/low temperature and low salt/high temperature, while it becomes apparent for other cases. At high salt/low temperature, the RNA is already folded and its structure is rather compact, and consequently a spatial confinement cannot cause the formation of more base pairs. For the other limit case of low salt/high temperature, the formation of base pairs would experience very strong electrostatic intra-chain repulsion and strong chain conformational entropy penalty, and the RNA chain would keep unfolded even in the presence of a spatial confinement; see **Supplementary Figure 3**. In the ranges of salt and temperature where the RNA is (partially) unfolded and the entropic penalty for base pairing/intra-chain
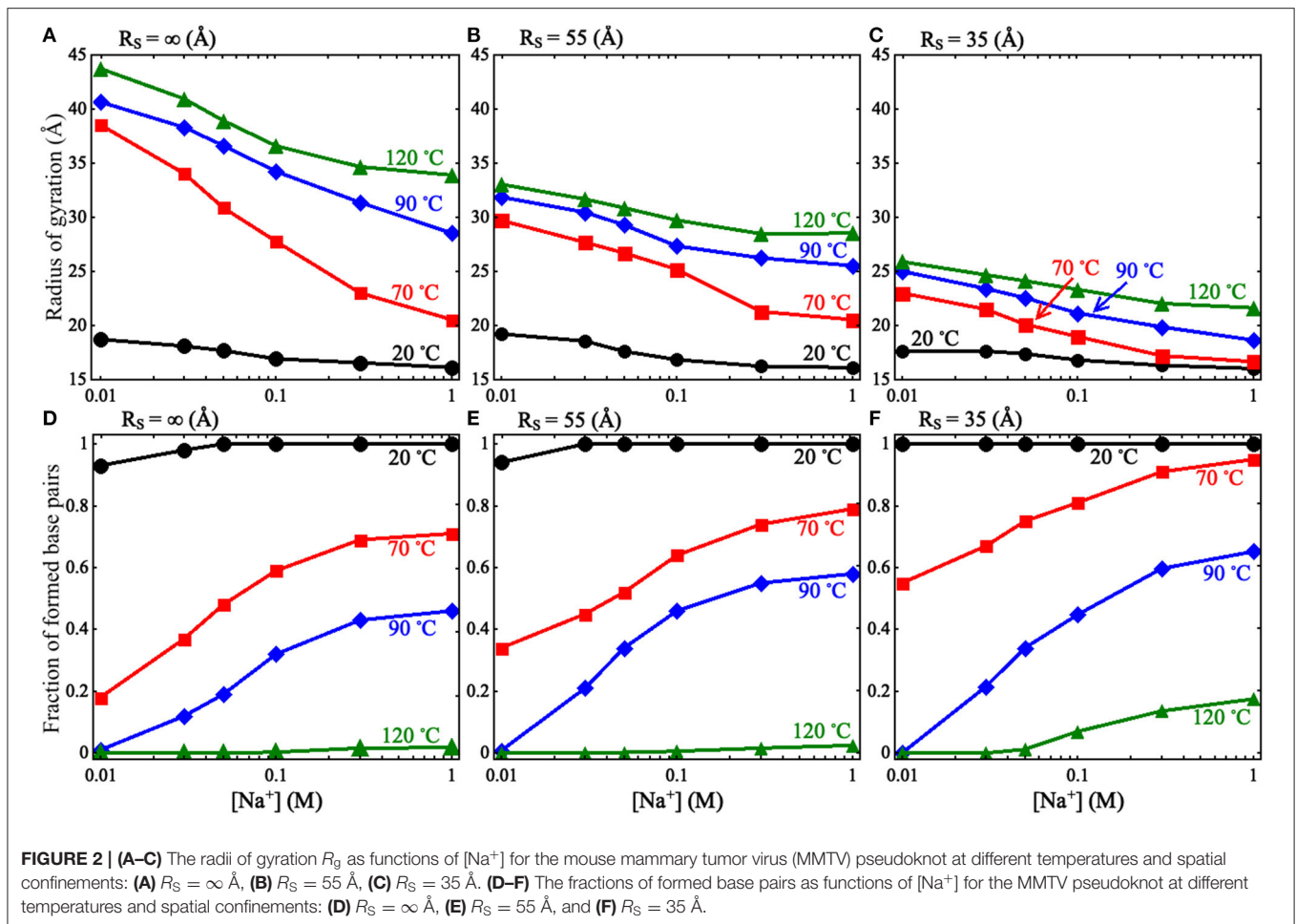
FIGURE 2 | (A–C) The radii of gyration R_g as functions of [Na$^+$] for the mouse mammary tumor virus (MMTV) pseudoknot at different temperatures and spatial confinements: **(A)** $R_S = \infty$ Å, **(B)** $R_S = 55$ Å, **(C)** $R_S = 35$ Å. **(D–F)** The fractions of formed base pairs as functions of [Na$^+$] for the MMTV pseudoknot at different temperatures and spatial confinements: **(D)** $R_S = \infty$ Å, **(E)** $R_S = 55$ Å, and **(F)** $R_S = 35$ Å.
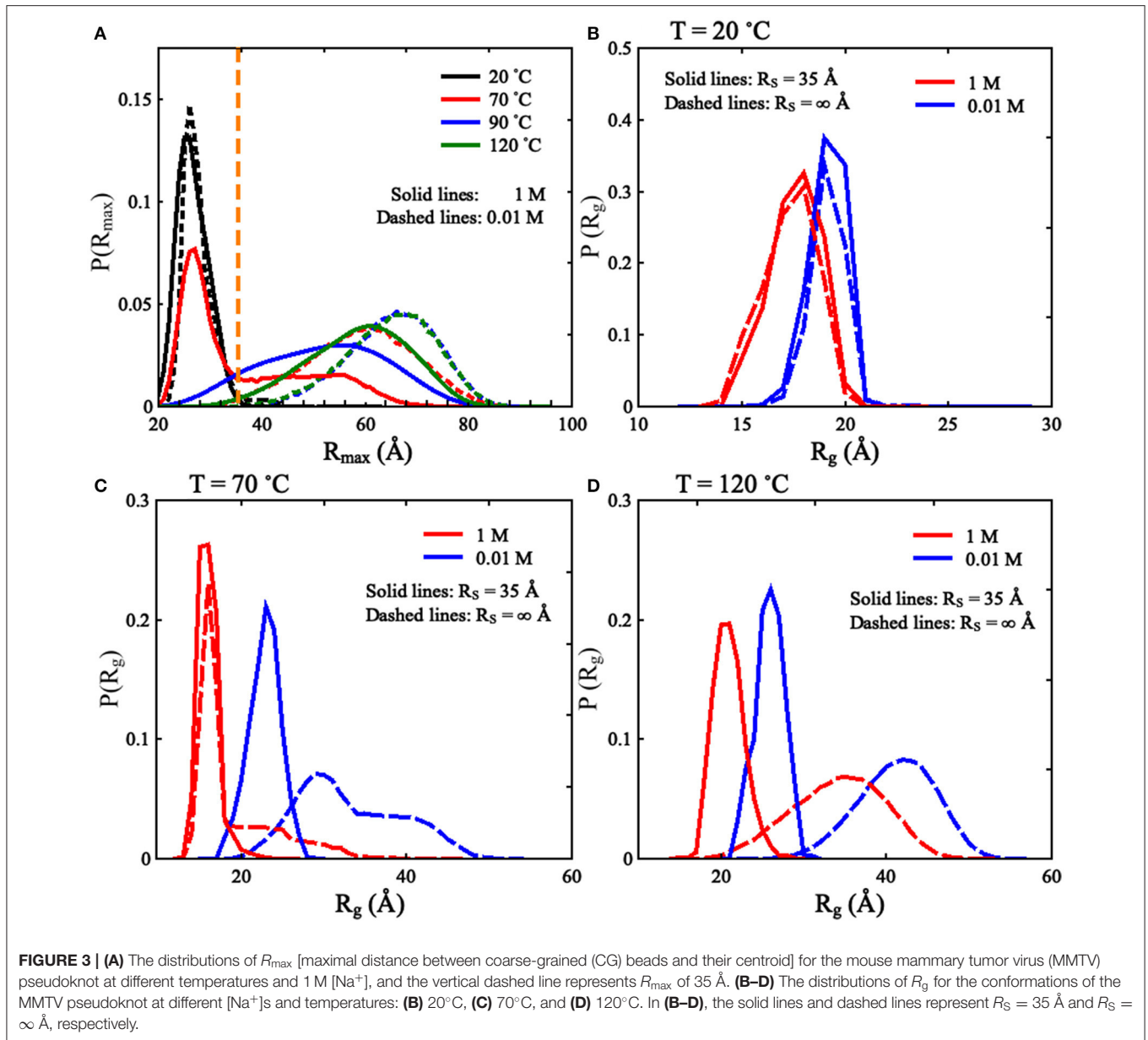
electrostatic repulsion is not strong, a spatial confinement can have an apparent effect on promoting base pairing in the RNA.

Effect of Spatial Confinement on Salt-Dependent Stability

We further examined the stability of the MMTV pseudoknot for different spatial confinements and ion conditions. During analyzing the unfolding of the pseudoknot, for each condition [i.e., (Na$^+$) and R_S], we performed one long-time simulation for the pseudoknot with enough conformations in equilibrium, and all the equilibrium conformations at different temperatures were used to analyze the RNA unfolding including melting temperatures and unfolding pathways; see **Supplementary Figures 2–5**. As shown in **Supplementary Figures 5A,B**, there are mainly three states that can be defined based on the number of base pairs at different temperatures: the fully folded pseudoknotted state (F), the intermediate hairpin states (I), and the unfolded coil state (U). And afterward, for each condition, the fractions of the F state and U state at different temperatures could be calculated, respectively, and fitted to a two-state model to obtain the two melting temperatures (T_{m1} and T_{m2}) for the

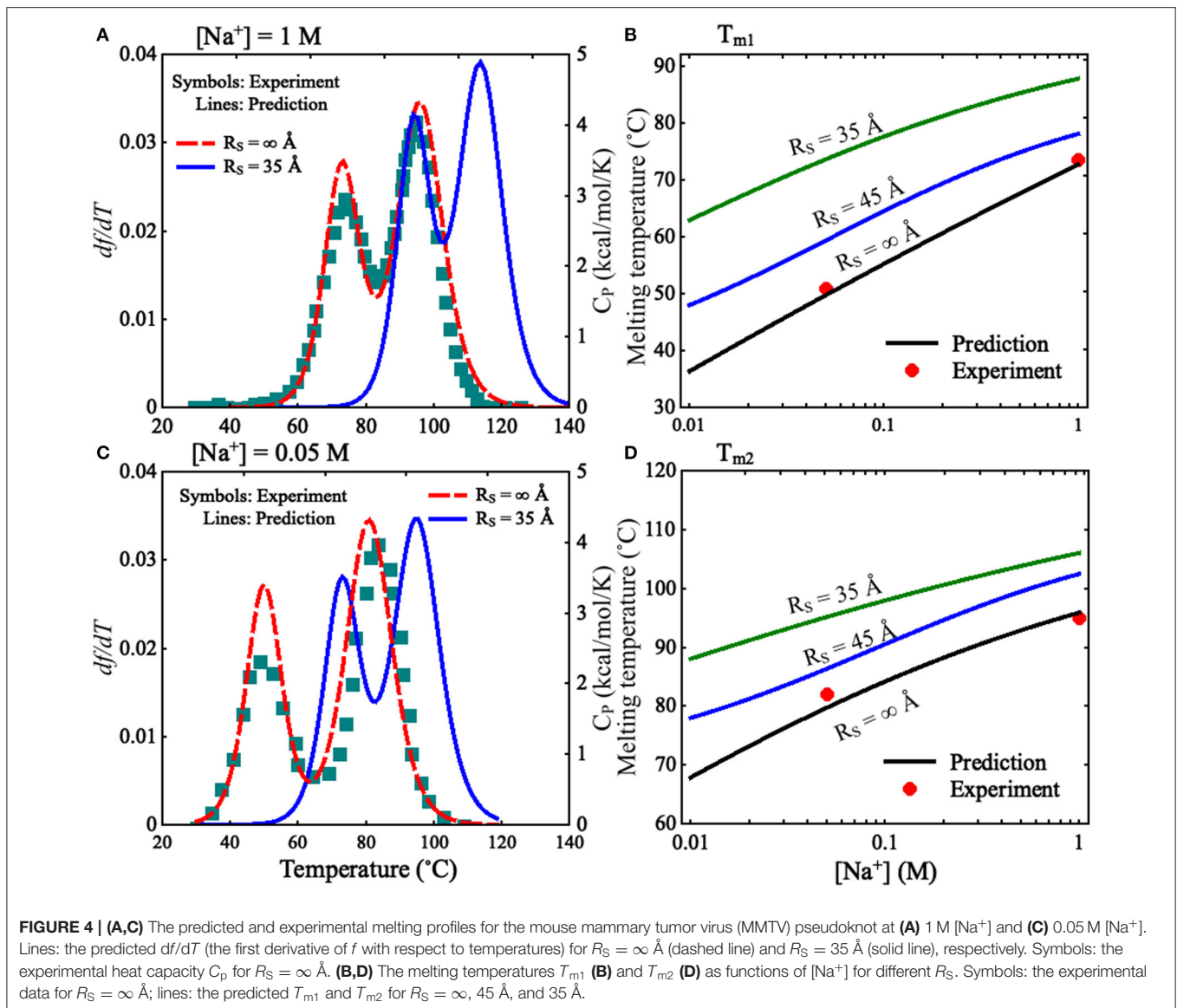corresponding transitions (F→I and I→U); for more details, refer **Supplementary Material** and Shi et al. (2018).

To validate the present model, we first predicted the melting temperatures for the pseudoknot at 1 M [Na$^+$] and 0.05 M [Na$^+$] in the absence of spatial confinement (i.e., $R_S = \infty$ Å) and then made the comparisons with the available experiment data (Shen and Tinoco, 1995). As shown in **Figures 4B,D**, the mean variation between the predicted and experimental T_ms (T_{m1} and T_{m2}) of the pseudoknot is <2°C, which indicates that the present model is reliable on predicting the stability of the pseudoknot at various salt concentrations. **Figures 4B,D** also shows that the stability of the pseudoknot can be significantly enhanced not only by the increase of [Na$^+$] but also by the involvement of the spatial confinement. For example, the two melting temperatures (T_{m1} and T_{m2}) of the pseudoknot increase from ~36 and 68°C to ~73 and 96°C, respectively, when [Na$^+$] is increased from 0.01 to 1 M in the absence of spatial confinement, and they increase from ~73 and 96°C to ~88 and 106°C, respectively, when the spatial confinement with $R_S = 35$ Å is involved at 1 M [Na$^+$]; see **Figures 4B,D**. Such salt-enhanced stability of the pseudoknot is attributed to the stronger ion neutralization effect at high salt (Tan and Chen, 2011; Shi et al., 2018). The enhancement effect of spatial confinement on the stability is because the

FIGURE 3 | (A) The distributions of R_{max} [maximal distance between coarse-grained (CG) beads and their centroid] for the mouse mammary tumor virus (MMTV) pseudoknot at different temperatures and 1 M [Na⁺], and the vertical dashed line represents R_{max} of 35 Å. **(B–D)** The distributions of R_g for the conformations of the MMTV pseudoknot at different [Na⁺]s and temperatures: **(B)** 20°C, **(C)** 70°C, and **(D)** 120°C. In **(B–D)**, the solid lines and dashed lines represent $R_S = 35$ Å and $R_S = \infty$ Å, respectively.

spatial confinement can effectively limit the conformational space and such effect is more pronounced for the more extended unfolded/partially unfolded state (Denesyuk and Thirumalai, 2011), for example, R_{max} of the U state at 1 M [Na⁺] will shrink from ~61 to ≤35 Å as the spatial confinement ($R_S = 35$ Å) is involved; see **Figure 5A**.

We also calculated the increase of melting temperatures due to the involvement of the confinement of $R_S = 35$ Å for the two transitions of F→I and I→U, which are denoted by $\Delta T_{m1,2}(R_S = 35$ Å$) = T_{m1,2}(R_S = 35$ Å$)-T_{m1,2}(R_S = \infty)$. $\Delta T_{m1}(R_S = 35$ Å$)$ (~15.0°C) for the F→I transition is slightly larger than $\Delta T_{m2}(R_S = 35$ Å$)$ (~10.0°C) for the I→U transition at 1 M [Na⁺]; see **Figure 4** and **Supplementary Figure 6**. This indicates that the spatial confinement could enhance the stability

of pseudoknotted state more strongly relative to corresponding intermediate (hairpin) state for the pseudoknot. This finding seems somewhat inconsistent with the recent study on the stability of the pseudoknot in human telomerase RNA under crowded conditions (Denesyuk and Thirumalai, 2011), and it is understandable. As shown in **Figure 5A**, for the pseudoknot at 1 M [Na⁺] without spatial confinement, we calculated the maximum distance R_{max} between CG beads and the centroid of each conformation. The distribution of R_{max} of the I state is only slightly more compact than that of the U state due to the small hairpin and very long tail in the I state, while it is significantly more extended than that of the F state. Thus, for the pseudoknot studied here, the spatial confinement can stabilize the folded state more strongly than the intermediate state through significantly

FIGURE 4 | (A,C) The predicted and experimental melting profiles for the mouse mammary tumor virus (MMTV) pseudoknot at **(A)** 1 M [Na$^+$] and **(C)** 0.05 M [Na$^+$]. Lines: the predicted df/dT (the first derivative of f with respect to temperatures) for $R_S = \infty$ Å (dashed line) and $R_S = 35$ Å (solid line), respectively. Symbols: the experimental heat capacity C_p for $R_S = \infty$ Å. **(B,D)** The melting temperatures T_{m1} **(B)** and T_{m2} **(D)** as functions of [Na$^+$] for different R_S. Symbols: the experimental data for $R_S = \infty$ Å; lines: the predicted T_{m1} and T_{m2} for $R_S = \infty$, 45, and 35 Å.

reducing the volume accessible for the extended unfolded state and slightly less extended intermediate state.

Furthermore, we examined the effect of spatial confinement on the salt-dependent stability of the pseudoknot. As shown in **Figures 4B,D**, the salt dependence of the stability for the pseudoknot can be apparently weakened by the spatial confinement for both of the transitions. For example, the increase of T_{m1} (~25°C) due to the increase of [Na$^+$] from 0.01 to 1 M for the confinement of $R_S = 35$ Å is apparently smaller than that of (~37°C) for $R_S = \infty$ Å, and similarly, the increase of T_{m2} (~18°C) with the increase of [Na$^+$] from 0.01 to 1 M for the confinement of $R_S = 35$ Å is apparently smaller than that of (~28°C) for $R_S = \infty$ Å. Such weakened salt dependence of the stability by spatial confinement for the pseudoknot is understandable. Physically, the spatial confinement can restrict the conformations of RNAs, and such effect is more pronounced

for more extended structures; see **Figure 5**. This causes that the unfolded U (or intermediate I) state becomes closer to the intermediate I (or folded F) state in structure compactness and consequently in charge density. Thus, the spatial confinement results in a weaker salt dependence of the stability of the pseudoknot for both of the F→I and I→U transitions due to the decreased differences in charge density between the F and I states and between the I and U states, respectively.

Effect of Spatial Confinement on Salt-Dependent Unfolding Pathway

Because of the importance of the unfolding pathway of RNA pseudoknots (Roca et al., 2018; Shi et al., 2018), we made further comprehensive analyses for the pseudoknot at different conditions to examine the effect of spatial confinement on the
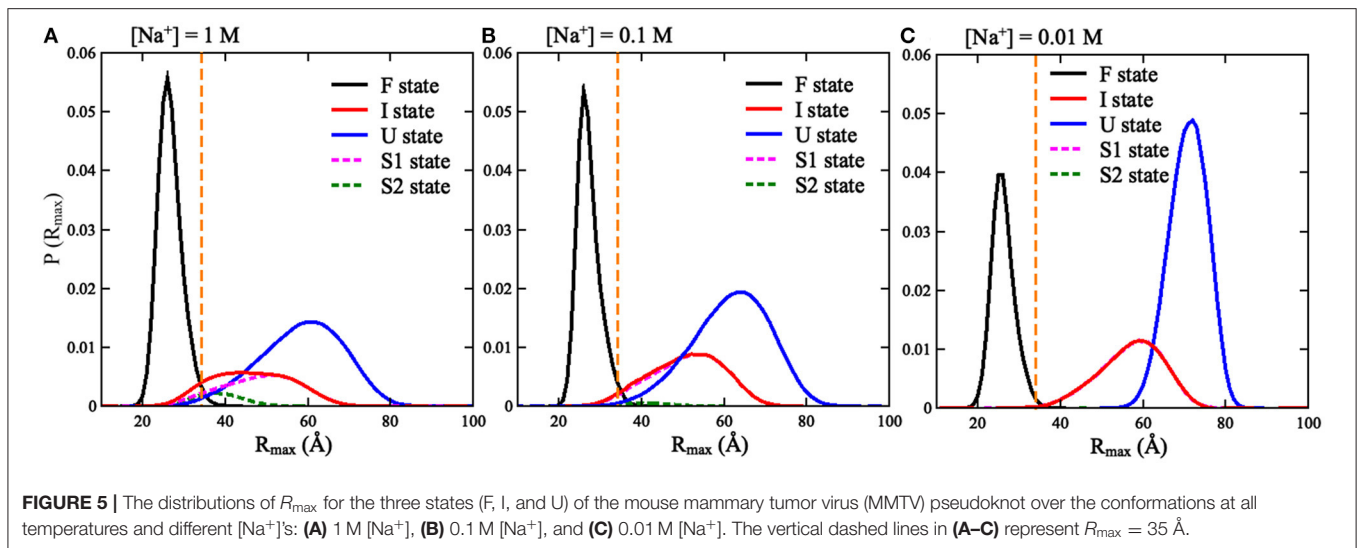
FIGURE 5 | The distributions of R_{max} for the three states (F, I, and U) of the mouse mammary tumor virus (MMTV) pseudoknot over the conformations at all temperatures and different [Na$^+$]'s: **(A)** 1 M [Na$^+$], **(B)** 0.1 M [Na$^+$], and **(C)** 0.01 M [Na$^+$]. The vertical dashed lines in **(A–C)** represent R_{max} = 35 Å.

unfolding pathway. Based on the simulations for the pseudoknot at a given (temperature and salt) condition, the I state can also be divided into two independent hairpin states: S1 and S2, with only Stem 1 or Stem 2, respectively; see **Figure 1**, and the fractions of S1 and S2 states can also be calculated at any condition including salt condition and spatial confinement. As shown in **Figure 6** for the factions of different states and **Figure 7** for the illustration of unfolding pathway, in the absence of spatial confinement ($R_S = \infty$ Å), the maximum fractions of the S1 and S2 states are ~70 and 20% at 1 M [Na$^+$], respectively, and changes into ~89 and 0% when [Na$^+$] is decreased from 1 M to 0.01 M. This indicates that the pseudoknot has two unfolding pathways at high salt: the major one of F→S1→U and the minor one of F→S2→U, which can be dramatically modulated into the only one pathway of F→S1→U by low salt. Such prediction agrees well with the recent experiments (Shen and Tinoco, 1995; Roca et al., 2018), and the unfolding pathway is determined by the relative stability between the S1 and S2 states, which can be changed by ions due to the different sizes of hairpins in S1 and S2 states (Shi et al., 2018). As shown in **Figure 7**, compared with the S1 state, the S2 state has a larger hairpin and consequently becomes less stable with the decrease of [Na$^+$] due to the stronger intra-chain electrostatic repulsion at lower [Na$^+$] (Tan and Chen, 2007, 2011).

Furthermore, as shown in **Figures 6**, **7**, a spatial confinement can also greatly influence the unfolding pathway of the pseudoknot at high salt concentrations, for example, at 1 M [Na$^+$], the maximal fractions of S1 and S2 states change from ~70 and 20% to ~35 and 30% when the spatial confinement with R_S of 35 Å is introduced; see **Figures 6C,F**. Such effect of spatial confinement is reasonable. As shown in **Figure 5A**, there is a significant difference in R_{max} distribution between two intermediate (S1 and S2) hairpin states at 1 M [Na$^+$]. The mean of R_{max} of S1 state (~52 Å) is apparently larger than that of S2 state (~37 Å) due to the longer tail in the S1 state. The result indicates that the S1 state with large size could be more strongly suppressed by the spatial confinement than the S2 state, and consequently, the fraction of S1 state would be reduced by the

spatial confinement. In contrast, the S2 state, with the majority of R_{max} close to the radius of spherical cavity (i.e., R_S = 35 Å), could be weakly suppressed by the spatial confinement and accordingly, the fraction of the S2 state can increase due to the apparent decreased fraction of the other intermediate (S1) state. Very importantly, the spatial confinement brings an apparent appearance of intermediate state of S1 state with additional base pairs in tail (e.g., U$_{22}$-G$_{29}$ and C$_{23}$-G$_{28}$). Here, we defined this new state including Stem 1 and additional base pairs in 3'-end as the S1V state, which can be considered a variant of S1 state. As shown in **Figure 6**, the spatial confinement of R_S = 35 Å causes the increase of the fraction of S1V state from ~0.9 to 6% at 1 M [Na$^+$]. The apparent appearance of S1V state is attributed to the compacting effect on the long tail of S1 state by the spatial confinement. In contrast to high salt, the spatial confinement has little effect on the unfolding pathway at low salt, and there is still only unfolding pathway of F→S1→U at low salt even in the presence of the spatial confinement of R_S = 35 Å. This is because the strong intra-chain electrostatic repulsion counteracts the effect of spatial confinement at low salt.

The above analyses for the pseudoknot indicate that the unfolding pathway of RNAs generally could be modulated by both ion conditions and spatial confinement. In **Figure 7**, we summarized the unfolding pathway of the pseudoknot in the presence of spatial confinement. At low salt, the pseudoknot has only one unfolding pathway in the presence/absence of spatial confinement. However, at high salt, the spatial confinements cause two major unfolding pathways with similar fractions and a new minor pathway through the S1 variant, in contrast to one major and one minor pathways in the absence of spatial confinement.

CONCLUSIONS

Motivated by the correlations between crowded cell environments and functions of RNA molecules, we examined
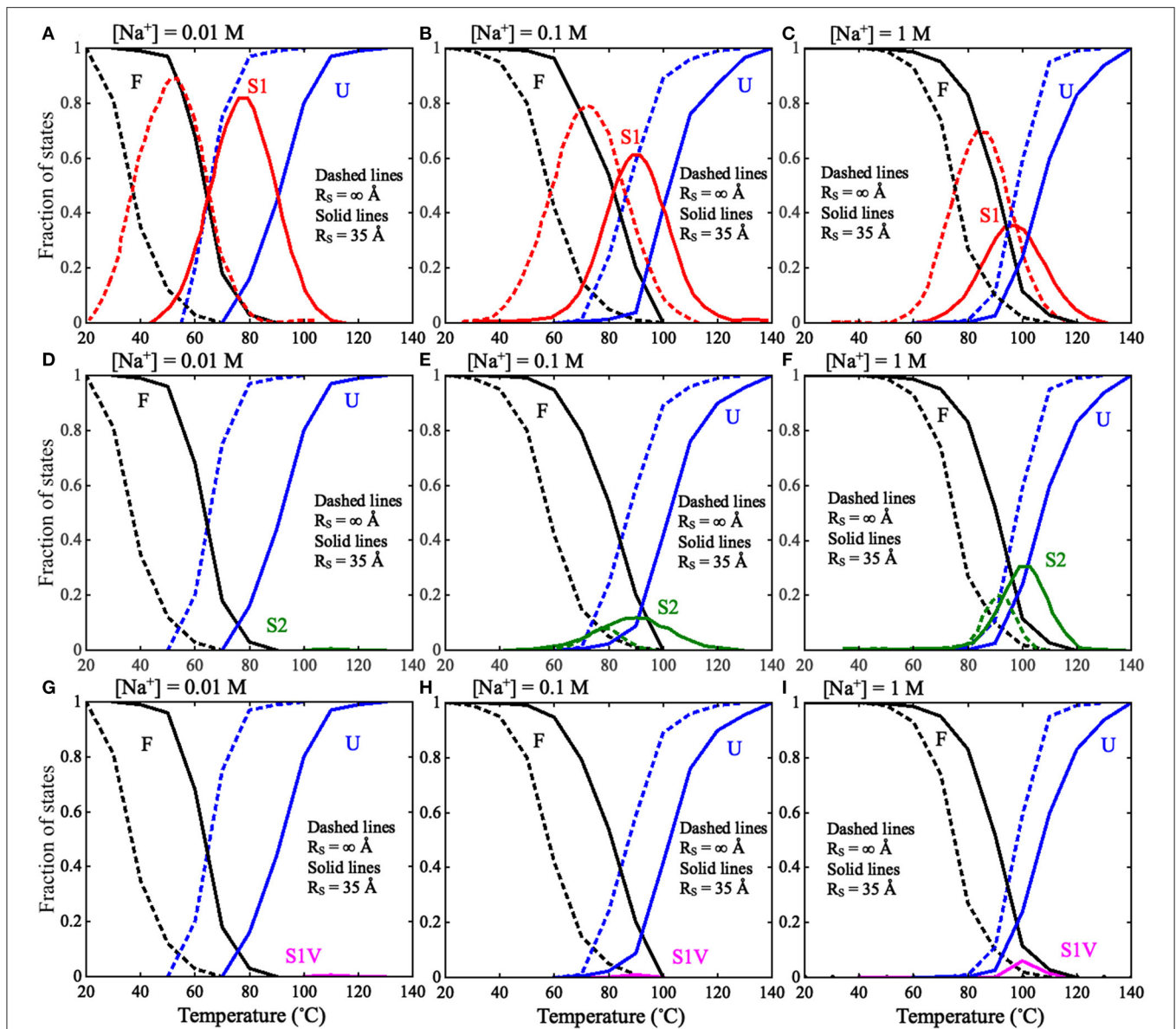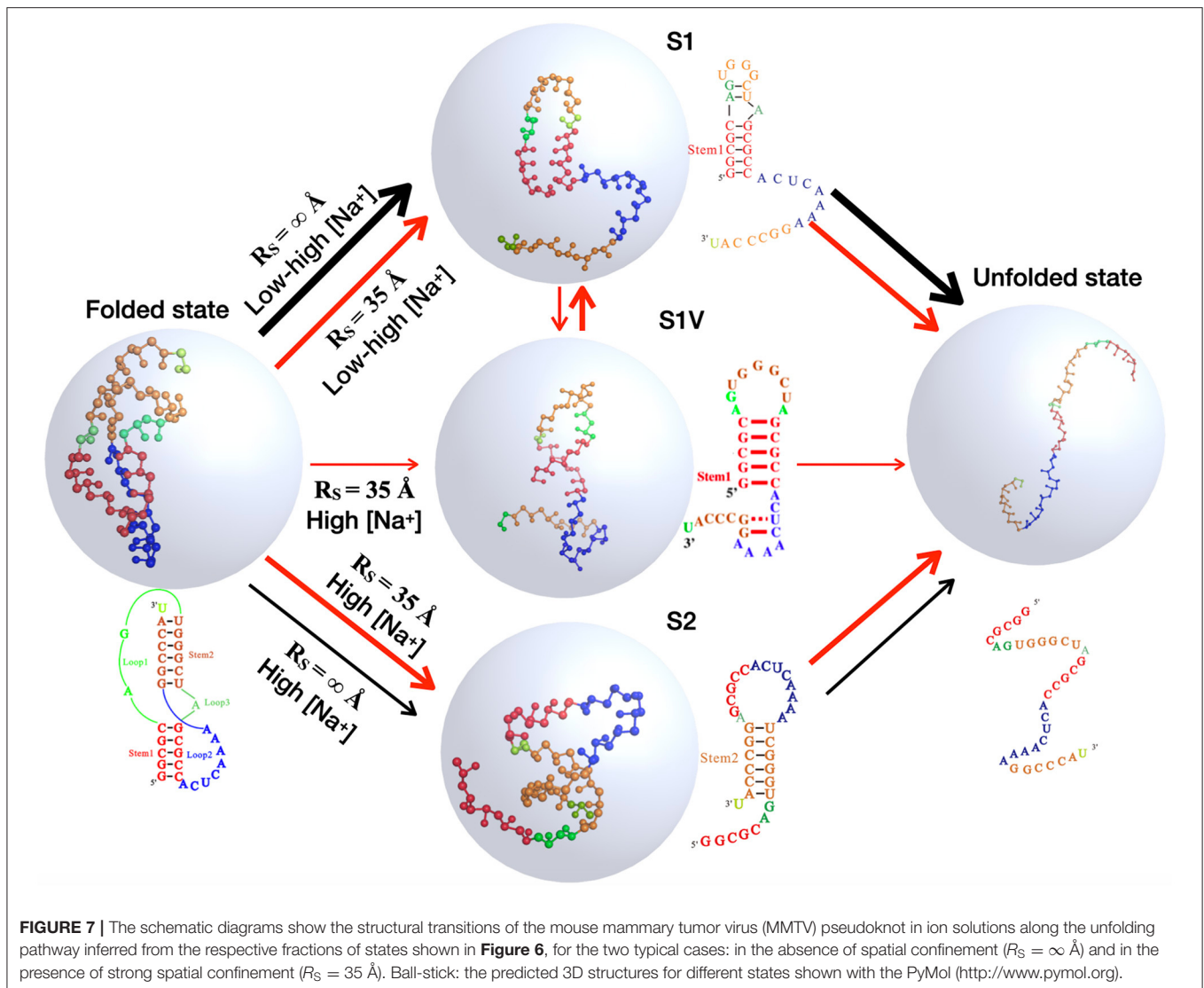
FIGURE 6 | The fractions of F, S1, S2, S1V, and U states as functions of temperature in thermal unfolding of the mouse mammary tumor virus (MMTV) pseudoknot for $R_S = \infty$ Å (dashed lines) and $R_S = 35$ Å (solid lines): **(A–C)** The fractions of F, S1, and U states at **(A)** 0.01 M [Na$^+$], **(B)** 0.1 M [Na$^+$], and **(C)** 1 M [Na$^+$]. **(D–F)** The fractions of F, S2, and U states at **(D)** 0.01 M [Na$^+$], **(E)** 0.1 M [Na$^+$], and **(F)** 1 M [Na$^+$]. **(G–I)** The fractions of F, S1V, and U states at **(A)** 0.01 M [Na$^+$], **(B)** 0.1 M [Na$^+$], and **(C)** 1 M [Na$^+$]. F stands for fully folded RNA, S1 stands for hairpin intermediate with Stem 1, S2 stands for hairpin intermediate with Stem 2, S1V stands for Stem1 variation, and U stands for fully unfolded RNA.

the effect of spatial confinement on the salt dependence of 3D structure, thermal stability, and unfolding pathway for the MMTV pseudoknot using our previously developed CG model for RNAs. First, based on the predicted 3D structures of the pseudoknot under different spatial confinements from its sequence, we found that the spatial confinement can weaken the dependence of 3D structure compactness on salt through severely restricting the extended RNA conformations at low ion concentrations or at high temperatures. Second, the spatial confinement can enhance the thermal stability of the RNA

structures, and such enhancement is more pronounced for low salt, causing that the spatial confinement can apparently weaken the dependence of stability on salt for both the pseudoknotted and intermediate hairpin states. This is attributed to the stabilizing effect of the spatial confinement is more pronounced for more extended (partially) denatured states at low salt. Finally, the unfolding pathway of the pseudoknot can be modulated by both ion conditions and spatial confinements. At low salt, the pseudoknot has only one unfolding pathway in the presence/absence of spatial confinement. However, at

FIGURE 7 | The schematic diagrams show the structural transitions of the mouse mammary tumor virus (MMTV) pseudoknot in ion solutions along the unfolding pathway inferred from the respective fractions of states shown in **Figure 6**, for the two typical cases: in the absence of spatial confinement ($R_S = \infty$ Å) and in the presence of strong spatial confinement ($R_S = 35$ Å). Ball-stick: the predicted 3D structures for different states shown with the PyMol (http://www.pymol.org).

high salt, the spatial confinements cause two major unfolding pathways with similar fractions and a new minor pathway, in contrast to one major and one minor pathways in the absence of spatial confinement.

Although we made reliable predictions and comprehensive analyses on salt-dependent structure stability for the MMTV pseudoknot under different spatial confinements, the effect of spatial confinement on structure stability for extensive RNA pseudoknots with various sequences/lengths and functional RNAs with complex structures (e.g., tRNA and riboswitches) in ion solutions should be studied by further developing the present CG model (Zhang et al., 2011; Kilburn et al., 2016; Yamagami et al., 2018), and further development on the present model may need to take into account the tertiary contacts beyond the canonical and wobble base pairs already involved in the model (Weinreb et al., 2016; Jian et al., 2019; Wang and Zhao, 2020). Furthermore, there are some other physical and chemical factors that could affect how crowding modulates RNA stability, which is beyond the approximation of the

spatial confinement considered here (Zhou et al., 2008; Nakano et al., 2009; Paudel and Rueda, 2014; Strulson et al., 2014; Leamy et al., 2016, 2017; Feig et al., 2017). For example, recent studies showed that molecular crowders could not only stabilize the tertiary structures of macromolecules by excluded volume but also destabilize RNA secondary structures through the surface interactions and reduction in water activity (Zhou et al., 2008; Gao et al., 2016; Leamy et al., 2017). Moreover, the related works from Thirumalai et al. also indicated that small crowders can increase the stability of compact structures of human telomerase RNA to a greater extent than larger ones (Denesyuk and Thirumalai, 2011), and the crowders with attractive interactions with RNA bases can stabilize an RNA hairpin more than inert crowding agents of the same size (Pincus et al., 2008). In addition, the interaction between ions (especially multivalent ion) and RNAs can be influenced by crowders (Yu et al., 2016), which is beyond the implicit ion treatment presented here and is required to be addressed in the future work (Tan and Chen, 2007, 2012; Xu and Chen, 2020).

Thus, to effectively simulate the RNA folding in the cellular environment with ions and different crowding macromolecules is still an important issue required to be solved. Nevertheless, this work could be very helpful for understanding the salt-dependent structure and stability for RNAs in cellular-like confined environment.

DATA AVAILABILITY STATEMENT

The original contributions presented in the study are included in the article/**Supplementary Material**, further inquiries can be directed to the corresponding author/s.

AUTHOR CONTRIBUTIONS

Z-JT, Y-ZS, and CF designed the research. CF and Y-ZS performed the simulations. Z-JT, CF, Y-LT, and Y-XC analyzed the data. CF, Y-ZS, and Z-JT wrote the manuscript. All authors discussed the results and reviewed the manuscript.

SUPPLEMENTARY MATERIAL

The Supplementary Material for this article can be found online at: https://www.frontiersin.org/articles/10.3389/fmolb.2021.666369/full#supplementary-material

REFERENCES

Boniecki, M. J., Lach, G., Dawson, W. K., Tomala, K., Lukasz, P., Soltysinski, T., et al. (2016). SimRNA: a coarse-grained method for RNA folding simulations and 3D structure prediction. *Nucleic Acids Res*. 44:e63. doi: 10.1093/nar/gkv1479

Cao, S., and Chen, S. J. (2005). Predicting RNA folding thermodynamics with a reduced chain representation model. *RNA* 11:1884. doi: 10.1261/rna.2109105

Cheung, M. S., Klimov, D., and Thirumalai, D. (2005). Molecular crowding enhances native state stability and refolding rates of globular proteins. *Proc. Natl. Acad. Sci. U.S.A*. 102, 4753–4758. doi: 10.1073/pnas.0409630102

Cragnolini, T., Laurin, Y., Derreumaux, P., and Pasquali, S. (2015). Coarse-grained HiRE-RNA model for ab initio RNA folding beyond simple molecules, including noncanonical and multiple base pairings. *J. Chem. Theory Comput*. 11, 3510–3522. doi: 10.1021/acs.jctc.5b00200

Das, R., Karanicolas, J., and Baker, D. (2010). Atomic accuracy in predicting and designing noncanonical RNA structure. *Nat. Methods* 7, 291–294. doi: 10.1038/nmeth.1433

Das, R., Travers, K. J., Bai, Y., and Herschlag, D. (2005). Determining the Mg^{2+} stoichiometry for folding an RNA metal ion core. *J. Am. Chem. Soc*. 127, 8272–8273. doi: 10.1021/ja051422h

Dawson, W. K., Maciejczyk, M., Jankowska, E. J., and Bujnicki, J. M. (2016). Coarse-grained modeling of RNA 3D structure. *Methods* 2016, 138–156. doi: 10.1016/j.ymeth.2016.04.026

Denesyuk, N. A., and Thirumalai, D. (2011). Crowding promotes the switch from hairpin to pseudoknot conformation in human telomerase RNA. *J. Am. Chem. Soc*. 133, 11858–11861. doi: 10.1021/ja2035128

Ding, F., Sharma, S., Chalasani, P., Demidov, V. V., and Broude, N. E. (2008). Ab initio RNA folding by discrete molecular dynamics: from structure prediction to folding mechanisms. *RNA* 14, 1164–1173. doi: 10.1261/rna.894608

Draper, D. E., Grilley, D., and Soto, A. M. (2005). Ions and RNA folding. *Annu. Rev. Biophys. Biomol. Struct*. 34, 221–243. doi: 10.1146/annurev.biophys.34.040204.144511

Dupuis, N. F., Holmstrom, E. D., and Nesbitt, D. J. (2014). Molecular-crowding effects on single-molecule RNA folding/unfolding thermodynamics and kinetics. *Proc. Natl. Acad. Sci. U.S.A*. 111, 8464. doi: 10.1073/pnas.1316039111

Feig, M., Yu, I., Wang, P. H., Nawrocki, G., and Sugita, Y. (2017). Crowding in cellular environments at an atomistic level from computer simulations. *J. Phys. Chem. B* 121, 8009–8025. doi: 10.1021/acs.jpcb.7b03570

Gao, M., Gnutt, D., Orban, A., Appel, B., Righetti, F., Winter, R., et al. (2016). RNA hairpin folding in the crowded cell. *Angew. Chem. Int. Ed*. 55, 3224–3228. doi: 10.1002/anie.201510847

Giedroc, D. P., and Cornish, P. V. (2009). Frameshifting RNA pseudoknots: structure and mechanism. *Virus Res*. 139, 193–208. doi: 10.1016/j.virusres.2008.06.008

Giedroc, D. P., Theimer, C. A., and Nixon, P. L. (2000). Structure, stability and function of RNA pseudoknots involved in stimulating ribosomal frameshifting. *J. Mol. Biol*. 298, 167–185. doi: 10.1006/jmbi.2000.3668

Hajdin, C. E., Ding, F., Dokholyan, N. V., and Weeks, K. M. (2010). On the significance of an RNA tertiary structure prediction. *RNA* 16, 1340–1349. doi: 10.1261/rna.1837410

He, J., Wang, J., Tao, H., Xiao, Y., and Huang, S. Y. (2019). HNADOCK: a nucleic acid docking server for modeling RNA/DNA–RNA/DNA 3D complex structures. *Nucleic Acids Res*. 47, W35–W42. doi: 10.1093/nar/gkz412

He, Y., Liwo, A., and Scheraga, H. A. (2015). Optimization of a nucleic acids united-RESidue 2-point model (NARES-2P) with a maximum-likelihood approach. *J. Chem. Phys*. 143, 243111. doi: 10.1063/1.4932082

He, Y., Maciejczyk, M., Oldziej, S., Scheraga, H. A., and Liwo, A. (2013). Mean-field interactions between nucleic-acid-base dipoles can drive the formation of a double helix. *Phys. Rev. Lett*. 110:098101. doi: 10.1103/PhysRevLett.110.098101

Hori, N., Denesyuk, N. A., and Thirumalai, D. (2016). Salt effects on the thermodynamics of a frameshifting RNA pseudoknot under tension. *J. Mol. Biol*. 428, 2847–2859. doi: 10.1016/j.jmb.2016.06.002

Jian, Y., Wang, X., Qiu, J., Wang, H., Liu, Z., Zhao, Y., et al. (2019). DIRECT: RNA contact predictions by integrating structural patterns. *BMC Bioinformatics* 20:497. doi: 10.1186/s12859-019-3099-4

Jin, L., Shi, Y. Z., Feng, C. J., and Tan, Z. J. (2018). Modeling structure, stability, and flexibility of double-stranded RNAs in salt solutions. *Biophys. J*. 115, 1403–1416. doi: 10.1016/j.bpj.2018.08.030

Jin, L., Tan, Y. L., Wu, Y., Wang, X., Shi, Y. Z., and Tan, Z. J. (2019). Structure folding of RNA kissing complexes in salt solutions: predicting 3D structure, stability, and folding pathway. *RNA* 25, 1532–1548. doi: 10.1261/rna.071662.119

Kilburn, D., Behrouzi, R., Lee, H. T., Sarkar, K., Briber, R. M., and Woodson, S. A. (2016). Entropic stabilization of folded RNA in crowded solutions measured by SAXS. *Nucleic Acids Res*. 44, 9452. doi: 10.1093/nar/gkw597

Kilburn, D., Roh, J. H., Behrouzi, R., Briber, R. M., and Woodson, S. A. (2013). Crowders perturb the entropy of RNA energy landscapes to favor folding. *J. Am. Chem. Soc*. 135, 10055–10063. doi: 10.1021/ja4030098

Kilburn, D., Roh, J. H., Guo, L., Briber, R. M., and Woodson, S. A. (2010). Molecular crowding stabilizes folded RNA structure by the excluded volume effect. *J. Am. Chem. Soc*. 132, 8690–8696. doi: 10.1021/ja101500g

Kim, N., Liang, C., Elmetwaly, S., Jung, S., Curuksu, J., and Schlick, T. (2014). Graph-based sampling for approximating global helical topologies of RNA. *Proc. Nalt. Acad. Sci. U.S.A.* 111, 4079–4084. doi: 10.1073/pnas.1318893111

Klimov, D. K., Newfield, D., and Thirumalai, D. (2002). Simulations of β-hairpin folding confined to spherical pores using distributed computing. *Proc. Natl. Acad. Sci. U.S.A.* 99, 8019–8024. doi: 10.1073/pnas.072220699

Leamy, K. A., Assmann, A. M., Mathews, D. H., and Bevilacqua, P. (2016). Bridging the gap between in vitro and in vivo RNA folding. *Q. Rev. Biophys.* 49:e10. doi: 10.1017/S003358351600007X

Leamy, K. A., Yennawar, N. H., and Bevilacqua, P. C. (2017). Cooperative RNA folding under cellular conditions arises from both tertiary structure stabilization and secondary structure destabilization. *Biochemistry* 56, 3422–3433. doi: 10.1021/acs.biochem.7b00325

Li, J., Zhang, J., Wang, J., Li, W., and Wang, W. (2016). Structure prediction of RNA loops with a probabilistic approach. *PLoS Comput. Biol.* 12:e1005032. doi: 10.1371/journal.pcbi.1005032

Li, J., Zhu, W., Wang, J., Li, W., Gong, S., Zhang, J., et al. (2018). RNA3DCNN: local and global quality assessments of RNA 3D structures using 3D deep convolutional neural networks. *PLoS Comput. Biol.* 14:e1006514. doi: 10.1371/journal.pcbi.1006514

Lipfert, J., Doniach, S., Das, R., and Herschlag, D. (2014). Understanding nucleic acid-ion interactions. *Annu. Rev. Biochem.* 83, 19.1–19.29. doi: 10.1146/annurev-biochem-060409-092720

Liwo, A., Baranowski, M., Czaplewski, C., Golas, E., He, Y., Jagiela, D., et al. (2014). A unified coarse-grained model of biological macromolecules based on mean-field multipole-multipole interactions. *J. Mol. Model.* 20:2306. doi: 10.1007/s00894-014-2306-5

Liwo, A., Czaplewski, C., Sieradzan, A. K., Lubecka, E. A., Lipska, A. G., Golon, L., et al. (2020). "Scale-consistent approach to the derivation of coarse-grained force fields for simulating structure, dynamics, and thermodynamics of biopolymers," in *Progress in Molecular Biology and Translational Science*, eds B. Strodel and B. Barz (Academic Press), 73–122. doi: 10.1016/bs.pmbts.2019.12.004

Manning, G. S. (1978). The molecular theory of polyelectrolyte solutions with applications to the electrostatic properties of polynucleotides. *Q. Rev. Biophys.* 11, 179–246. doi: 10.1017/S0033583500002031

Meng, W., Timsina, R., Bull, A., Andresen, K., and Qiu, X. (2020). Additive modulation of DNA-DNA interactions by interstitial ions. *Biophys. J.* 118, 3019–3025. doi: 10.1016/j.bpj.2020.05.001

Mittal, J., and Best, R. B. (2008). Thermodynamics and kinetics of protein folding under confinement. *Proc. Natl. Acad. Sci. U.S.A.* 105, 20233–20238. doi: 10.1073/pnas.0807742105

Nakano, S. I., Karimata, H. T., Kitagawa, Y., and Sugimoto, N. (2009). Facilitation of RNA enzyme activity in the molecular crowding media of cosolutes. *J. Am. Chem. Soc.* 131, 16881–16888. doi: 10.1021/ja9066628

Parisien, M., and Major, F. (2008). The MC-Fold and MC-Sym pipeline infers RNA structure from sequence data. *Nature* 452, 51–55. doi: 10.1038/nature06684

Paudel, B. P., and Rueda, D. (2014). Molecular crowding accelerates ribozyme docking and catalysis. *J. Am. Chem. Soc.* 136, 16700–16703. doi: 10.1021/ja5073146

Pincus, D. L., Hyeon, C., and Thirumalai, D. (2008). Effects of trimethylamine N-Oxide (TMAO) and crowding agents on the stability of RNA hairpins. *J. Am. Chem. Soc.* 130, 7364–7372. doi: 10.1021/ja078326w

Popenda, M., Szachniuk, M., Antczak, M., Purzycka, K. J., Lukasiak, P., Bartol, N., et al. (2012). Automated 3D structure composition for large RNAs. *Nucleic Acids Res.* 40:e112. doi: 10.1093/nar/gks339

Qin, S., and Zhou, H. X. (2014). Further development of the FFT-based method for atomistic modeling of protein folding and binding under crowding: optimization of accuracy and speed. *J. Chem. Theory Comput.* 10, 2824–2835. doi: 10.1021/ct5001878

Qiu, X., Parsegian, V. A., and Rau, D. C. (2010). Divalent counterion-induced condensation of triple-strand DNA. *Proc. Natl. Acad. Sci. U.S.A.* 107, 21482–21486. doi: 10.1073/pnas.1003374107

Roca, J., Hori, N., Baral, S., Velmurugu, Y., Narayanan, R., Narayanan, P., et al. (2018). Monovalent ions modulate the flux through multiple folding pathways of an RNA pseudoknot. *Proc. Natl. Acad. Sci. U.S.A.* 115, e7313–e7322. doi: 10.1073/pnas.1717582115

Rose, P. W., Beran, B., Bi, C., Bluhm, W. F., Dimitropoulos, D., Goodsell, D. S., et al. (2011). The RCSB protein data bank: redesigned web site and web services. *Nucleic Acids Res.* 39, D392–D401. doi: 10.1093/nar/gkq1021

Sashital, D. G., and Doudna, J. A. (2010). Structural insights into RNA interference. *Curr. Opin. Struct. Biol.* 20, 90–97. doi: 10.1016/j.sbi.2009.12.001

Schlick, T., and Pyle, A. M. (2017). Opportunities and challenges in RNA structural modeling and design. *Biophys. J.* 113, 225–234. doi: 10.1016/j.bpj.2016.12.037

Serganov, A., and Patel, D. J. (2007). Ribozymes, riboswitches and beyond: regulation of gene expression without proteins. *Nat. Rev. Genet.* 8, 776–790. doi: 10.1038/nrg2172

Shen, L. X., and Tinoco, I. Jr. (1995). The structure of an RNA pseudoknot that causes efficient frameshifting in mouse mammary tumor virus. *J. Mol. Biol.* 247, 963–978. doi: 10.1006/jmbi.1995.0193

Shi, Y. Z., Jin, L., Feng, C. J., Tan, Y. L., and Tan, Z. J. (2018). Predicting 3D structure and stability of RNA pseudoknots in monovalent and divalent ion solutions. *PLoS Comput. Biol.* 14:e1006222. doi: 10.1371/journal.pcbi.1006222

Shi, Y. Z., Jin, L., Wang, F. H., Zhu, X. L., and Tan, Z. J. (2015). Predicting 3D structure, flexibility, and stability of RNA hairpins in monovalent and divalent ion solutions. *Biophys. J.* 109, 2654–2665. doi: 10.1016/j.bpj.2015.11.006

Shi, Y. Z., Wang, F. H., Wu, Y. Y., and Tan, Z. J. (2014a). A coarse-grained model with implicit salt for RNAs: predicting 3D structure, stability and salt effect. *J. Chem. Phys.* 141:105102. doi: 10.1063/1.4894752

Shi, Y. Z., Wu, Y. Y., Wang, F. H., and Tan, Z. J. (2014b). RNA structure prediction: progress and perspective. *Chin. Phys. B* 23:078701. doi: 10.1088/1674-1056/23/7/078701

Spasic, A., Berger, K. D., Chen, J. L., Seetin, M. G., Turner, D. H., and Mathews, D. H. (2018). Improving RNA nearest neighbor parameters for helices by going beyond the two-state model. *Nucleic Acids Res.* 46, 4883–4892. doi: 10.1093/nar/gky270

Staple, D. W., and Butcher, S. E. (2005). Pseudoknots: RNA structures with diverse functions. *PLoS Biol.* 3, 956–959. doi: 10.1371/journal.pbio.0030213

Strulson, C. A., Boyer, J. A., Whitman, E. E., and Bevilacqua, P. C. (2014). Molecular crowders and cosolutes promote folding cooperativity of RNA under physiological ionic conditions. *RNA* 20, 331–347. doi: 10.1261/rna.042747.113

Sulc, P., Romano, F., Ouldridge, T. E., Doye, J. P., and Louis, A. A. (2014). A nucleotide-level coarse-grained model of RNA. *J. Chem. Phys.* 140:235102. doi: 10.1063/1.4881424

Tan, Y. L., Feng, C. J., Jin, L., Shi, Y. Z., Zhang, W., and Tan, Z. J. (2019). What is the best reference state for building statistical potentials in RNA 3D structure evaluation? *RNA* 25, 793–812. doi: 10.1261/rna.069872.118

Tan, Z. J., and Chen, S. J. (2007). RNA helix stability in mixed Na^+/Mg^{2+} solution. *Biophys. J.* 92, 3615–3632. doi: 10.1529/biophysj.106.100388

Tan, Z. J., and Chen, S. J. (2010). Predicting ion binding properties for RNA tertiary structures. *Biophys. J.* 99, 1565. doi: 10.1016/j.bpj.2010.06.029

Tan, Z. J., and Chen, S. J. (2011). Salt contribution to RNA tertiary structure folding stability. *Biophys. J.* 101, 176. doi: 10.1016/j.bpj.2011.05.050

Tan, Z. J., and Chen, S. J. (2012). Ion-mediated RNA structural collapse: effect of spatial confinement. *Biophys. J.* 103, 827–836. doi: 10.1016/j.bpj.2012.06.048

Wang, H., and Zhao, Y. (2020). Methods and applications of RNA contact prediction. *Chin. Phys. B* 29, 108708. doi: 10.1088/1674-1056/abb7f3

Wang, J., Zhao, Y., Wang, J., and Xiao, Y. (2015a). Computational study of stability of an H-H-type pseudoknot motif. *Phys. Rev. E* 92:062705. doi: 10.1103/PhysRevE.92.062705

Wang, J., Zhao, Y., Zhu, C., and Xiao, Y. (2015b). 3dRNAscore: a distance and torsion angle dependent evaluation function of 3D RNA structures. *Nucleic Acids Res.* 43:e63. doi: 10.1093/nar/gkv141

Wang, Y., Wang, Z., Liu, T., Gong, S., and Zhang, W. (2018). Effects of flanking regions on HDV cotranscriptional folding kinetics. *RNA* 24, 1229–1240. doi: 10.1261/rna.065961.118

Wang, Y. J., Liu, T. G., Yu, T., Tan, Z. J., and Zhang, W. (2020). Salt effect on thermodynamics and kinetics of a single RNA base pair. *RNA* 26, 470–480. doi: 10.1261/rna.073882.119

Weinreb, C., Riesselman, A. J., Ingraham, J. B., Gross, T., Sander, C., and Marks, D. S. (2016). 3D RNA and functional interactions from evolutionary couplings. *Cell* 165, 963–975. doi: 10.1016/j.cell.2016.03.030

Xia, T., SantaLucia, J., Burkand, M. E., Kierzek, R., Schroeder, S. J., Jiao, X., et al. (1998). Thermodynamic parameters for an expanded nearest-neighbor model

for formation of RNA duplexes with watson-crick base pairs. *Biochemistry* 37, 14719–14735. doi: 10.1021/bi9809425

Xu, X., and Chen, S. J. (2020). Topological constraints of RNA pseudoknotted and loop-kissing motifs: applications to three-dimensional structure prediction. *Nucleic Acids Res*. 48, 6503–6512. doi: 10.1093/nar/gkaa463

Yamagami, R., Bingaman, J. L., Frankel, E. A., and Bevilacqua, P. C. (2018). Cellular conditions of weakly chelated magnesium ions strongly promote RNA stability and catalysis. *Nat. Commun*. 9:2149. doi: 10.1038/s41467-018-04415-1

Yu, T., Zhu, Y., He, Z., and Chen, S. J. (2016). Predicting molecular crowding effects in ion-RNA interactions. *J. Phys. Chem. B* 120, 8837–8844. doi: 10.1021/acs.jpcb.6b05625

Zhang, J., Dundas, J., Lin, M., Chen, R., Wang, W., and Liang, J. (2009). Prediction of geometrically feasible three-dimensional structures of pseudoknotted RNA through free energy estimation. *RNA* 15, 2248–2263. doi: 10.1261/rna.1723609

Zhang, Y., Zhang, J., and Wang, W. (2011). Atomistic analysis of pseudoknotted RNA unfolding. *J. Am. Chem. Soc*. 133, 6882–6885. doi: 10.1021/ja1109425

Zhao, Y. J., Huang, Y. Y., Gong, Z., Wang, Y. J., Man, J. F., and Xiao, Y. (2012). Automated and fast building of three-dimensional RNA structures. *Sci. Rep*. 2:734. doi: 10.1038/srep 00734

Zhou, H. X., Rivas, G. N., and Minton, A. P. (2008). Macromolecular crowding and confinement: biochemical, biophysical, and potential physiological consequences. *Annu. Rev. Biophys*. 37, 375–397. doi: 10.1146/annurev.biophys.37.032807.125817